AGU PUBLICATIONS

Geochemistry, Geophysics, Geosystems

RESEARCH ARTICLE
10.1002/2015GC006100

Structure of the mantle beneath the Alboran Basin from magnetotelluric soundings

X. Garcia[1], H. Seillé[2], J. Elsenbeck[3], R. L. Evans[3], M. Jegen[4], Sebastian Hölz[4], J. Ledo[5], A. Lovatini[6], A. Marti[5], A. Marcuello[5], P. Queralt[5], C. Ungarelli[6], and C. R. Ranero[7]

[1]Barcelona Center for Subsurface Imaging, Institute of Marine Sciences, CSIC, Barcelona, Spain, [2]Departament de Geodinàmica i Geofísica, Universitat de Barcelona, Barcelona, Spain, [3]Department of Geology and Geophysics, Woods Hole Oceanographic Institution, Woods Hole, Massachusetts, USA, [4]Helmholtz Centre for Ocean Research Kiel (GEOMAR), Geodynamics Department, Kiel, Germany, [5]Institut de Recerca Geomodels, Universitat de Barcelona, Barcelona, Spain, [6]Integrated EM Center of Excellence, Schlumberger Geosolutions, Milan, Italy, [7]ICREA at CSIC, Barcelona Center for Subsurface Imaging, Institute of Marine Sciences, CSIC, Barcelona, Spain

Key Points:
- First marine MT survey in Alboran, an area of very complex topography and tectonic history
- Two conductive anomalies are interpreted as fluids released from the Alboran subducting plate
- We imaged the subducting slab as a resistor that changes its electrical properties at 200 km depth

Supporting Information:
- Supporting Information S1

Correspondence to:
X. Garcia,
xgarcia@icm.csic.es

Citation:
Garcia, X., et al. (2015), Structure of the mantle beneath the Alboran Basin from magnetotelluric soundings, *Geochem. Geophys. Geosyst.*, *16*, 4261–4274, doi:10.1002/2015GC006100.

Received 17 SEP 2015
Accepted 11 NOV 2015
Accepted article online 14 NOV 2015
Published online 19 DEC 2015

Abstract We present results of marine MT acquisition in the Alboran sea that also incorporates previously acquired land MT from southern Spain into our analysis. The marine data show complex MT response functions with strong distortion due to seafloor topography and the coastline, but inclusion of high resolution topography and bathymetry and a seismically defined sediment unit into a 3-D inversion model has allowed us to image the structure in the underlying mantle. The resulting resistivity model is broadly consistent with a geodynamic scenario that includes subduction of an eastward trending plate beneath Gibraltar, which plunges nearly vertically beneath the Alboran. Our model contains three primary features of interest: a resistive body beneath the central Alboran, which extends to a depth of ~150 km. At this depth, the mantle resistivity decreases to values of ~100 Ohm-m, slightly higher than those seen in typical asthenosphere at the same depth. This transition suggests a change in slab properties with depth, perhaps reflecting a change in the nature of the seafloor subducted in the past. Two conductive features in our model suggest the presence of fluids released by the subducting slab or a small amount of partial melt in the upper mantle (or both). Of these, the one in the center of the Alboran basin, in the uppermost-mantle (20–30 km depth) beneath Neogene volcanics and west of the termination of the Nekkor Fault, is consistent with geochemical models, which infer highly thinned lithosphere and shallow melting in order to explain the petrology of seafloor volcanics.

1. Introduction

The westernmost Mediterranean is the locus of slow convergence between the Iberian and African plates and, as a result, is marked by complex tectonic activity. The processes dominating the local tectonics have long been debated with a range of models proposed including subduction with various geometries and delamination of lithospheric mantle [e.g., *Platt and Vissers*, 1989; *Lonergan and White*, 1997]. Current thinking suggests a model of subduction with an arcuate system but which has a plate that is dipping eastward beneath Gibraltar and then plunges nearly vertically beneath the Alboran Sea. Rollback of the slab plays a key part in the behavior of the Alboran domain and the formation of the surrounding Betic-Rif orocline [*Lonergan and White*, 1997; *Wortel and Spakman*, 2000; *Spakman and Wortel*, 2004; *Bezada et al.*, 2013; *Palomeras et al.*, 2014; *Thurner et al.*, 2014].

A good deal of our understanding of the mantle structure beneath the region comes from a range of seismic studies. Seismically active high-velocity lithosphere (either oceanic or subcontinental) is imaged extending beneath southern Spain and the Gibraltar arc in regional tomograms [*Bezada et al.*, 2013; *Wortel and Spakman*, 2000]. Because these structures extend down to the transition zone, they hold a record spanning several millions of years. The occurrence of intermediate-depth and deep earthquakes suggests the subduction of oceanic lithosphere [e.g., *Gutscher et al.*, 2002].

Global tomographic models appear to show a high P-wave velocity feature that is slab-like converging from the Atlantic and dipping to the east beneath Gibraltar before plunging beneath the Alboran [*Amaru*, 2007;

© 2015. American Geophysical Union. All Rights Reserved.

van Hinsbergen et al., 2014]. A widespread region of reduced velocities is seen in the upper mantle above the downgoing slab. More focused tomography, using an array of seismometers deployed throughout Spain, Morocco and including some seafloor instruments, confirms the presence of a high velocity anomaly with an arcuate structure that plunges nearly vertically beneath the Alboran through the 410 km discontinuity [*Bezada et al*., 2013]. Beneath the Alboran, velocities are high throughout the model.

A shear-wave velocity model derived from Rayleigh wave data also shows a high velocity anomaly centered beneath the Alboran from a depth of about 75 km [*Palomeras et al*., 2014]. This model has greater resolution within the crust and upper-mantle than does the teleseismic tomography model, and highlights a region of low velocities beneath Gibraltar with a peak low velocity anomaly magnitude at 50 km depth. Another low-velocity zone is coincident with a major strike-slip fault running through the Alboran [*Platt et al*., 2013], which has been interpreted by some to mark the plate boundary between the Alboran domain and the African plate. The low-velocity anomaly sits below Neogene volcanics mapped on the seafloor. Thermobarometric constraints on these volcanics indicate shallow depths (∼20 km) and high temperatures of melt equilibration, suggesting extremely thin lithosphere beneath the Alboran [*Thurner et al*., 2014]. Crustal thickness beneath these volcanics is thinner than the regional norm with a value of ∼20 km.

Geodynamic modeling has been used to determine which evolutionary history of competing subduction zone geometries are consistent with present-day observations [*Chertova et al*., 2014]. The model which is most consistent with the present-day tectonic framework and seismic images of the mantle began with a short subduction system with a ∼NW convergence near the Baleares in eastern Spain. This system split into two separate subduction systems, one jumping to the northern African coast, east of our survey area (Figure 1), and the other progressively rolling back through the Alboran until it achieved the arcuate structure seen today.

Dense coverage of SKS splitting data has been obtained throughout the region. The patterns of splitting are complex, but have an arcuate shape surrounding the Alboran [*Miller et al*., 2013]. Geodynamic modeling has been carried out to seek models that best reproduce the observed splitting patterns [*Alpert et al*., 2013]. The best fitting model contains an elongated slab (∼500 km wide) beneath the Iberian margin that curves southward on approach to Gibraltar. The slab is essentially a vertical structure in the mantle extending to a depth of ∼550 km, and best reproduces responses if it has a high viscosity compared to the surrounding mantle (a factor of 250 times more viscous).

Land magnetotelluric (MT) data in southern Spain have been previously used to image an area of low resistivity coincident with an area of low seismic velocities and with an absence of seismicity, interpreted as asthenospheric material intruded by the lateral lithospheric tearing and breaking-off of the east-directed subducting Ligurian slab under the Alboran Domain [*Rosell et al*., 2011]. Although controversial, this model is somewhat consistent with the structure of the slab inferred from seismic imaging, which shows a detachment of the slab from the lithosphere beneath southern Spain [*Thurner et al*., 2014]. This model is also consistent with results obtained by *Mancilla et al*. [2013] using geodetic and receiver transfer function analysis and with uplift rates necessary to explain sea-level changes in the Mediterranean and the Messinian Salinity Crisis [*García-Castellanos and Villaseñor*, 2011].

Marine Magnetotellurics (MMT) uses the same principal as land MT but requires instrumentation that can operate at high pressure on the seafloor. The techniques has been used by academia since the early 70s [e.g., *Filloux*, 1980] although more recently, in part due to interest in the method from industry [e.g., *Strack*, 2014], access to greater number of instruments with improved hardware has made the method a powerful tool for marine exploration that is complementary to seismic techniques [see e.g., *Baba*, 2005; *Worzewski et al*., 2010; *Key*, 2012; *Naif et al*., 2013].

2. Survey

As part of several international projects carried out in this area, MT methods have been used to explore the crust and upper mantle (Figure 1). We present results from a marine MT survey carried out in the Alboran Sea, but incorporating a subset of the land MT data previously collected in the Betic chain to better constrain the limits of the model and thus include all the structures that influence the measured data.

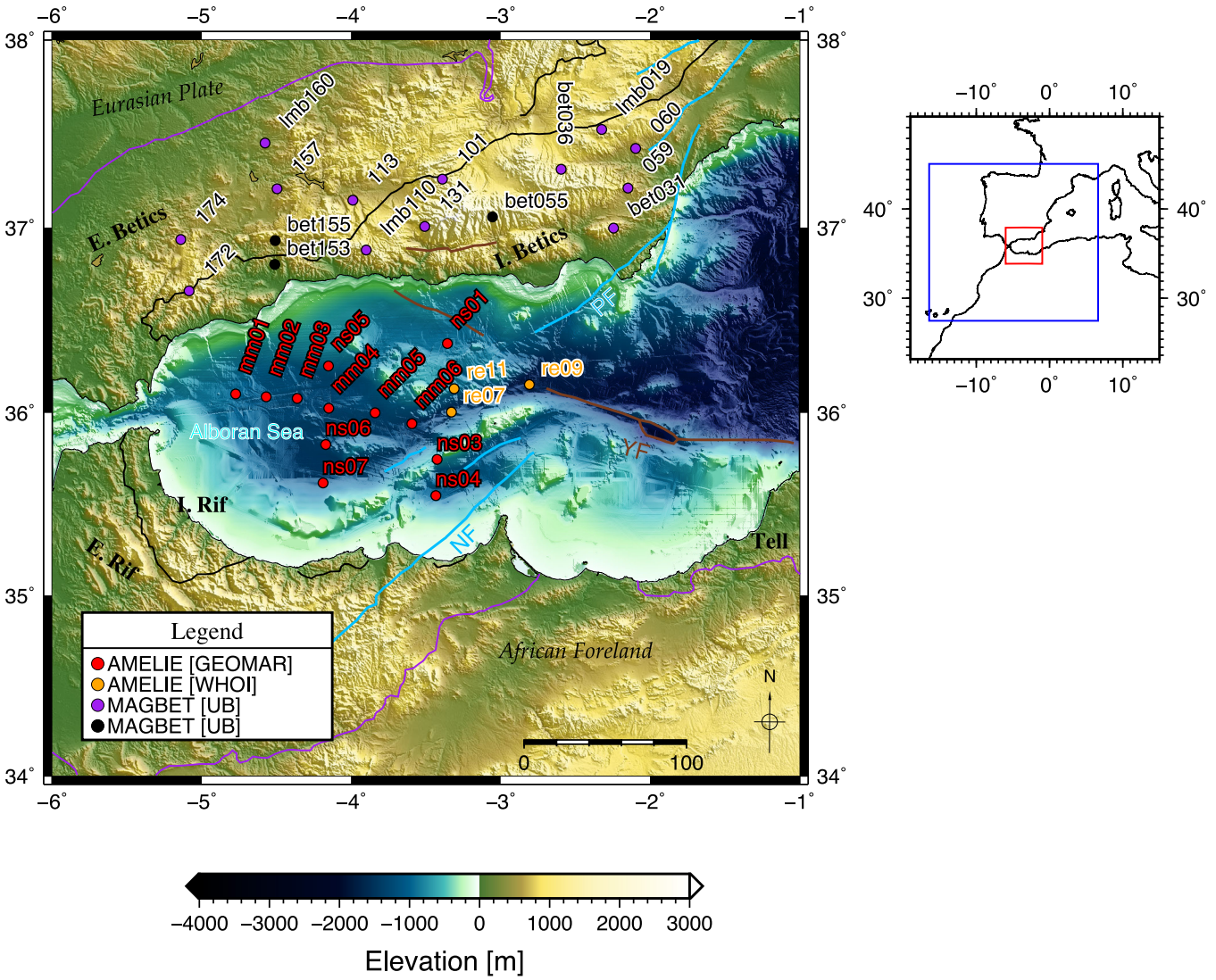

Figure 1. A map of the western Mediterranean showing all locations of MT stations used in this study. In black are sites that are not used in this study because of their low quality at the time of the inversions, although they will be used in a future inversion after being reprocessed. Main tectonic features (taking from *Platt et al.* [2013]) have been added to the plot, with purple lines indicating the boundaries of the Alboran slab, and in black the boundaries between the internal and external areas of Alboran subdomains. NF: Nekkor Fault. YF: Yussuf Fault. PF: Palomeras Fault. The inset plot on the right shows the extent of the map with site location in red and the actual extent of the 3-D mesh in blue.

The Alboran Sea has a highly variable bathymetry, extending to as deep as 2000 m. The region hosts an active fishing industry, with bottom trawling a common practice. As a result, no sites were deployed in water depths shallower than ∼800 m, typically the maximum depth of trawling. Despite this restriction, we were able to complete good coverage through the Alboran (Figure 1).

We successfully deployed and recovered 12 GEOMAR MMT instruments from August – December 2009, and 3 WHOI MMT instruments from November 2010 to March 2011. However, 5 additional instruments were lost, in most of the cases due to unknown reasons related to a failure in the acoustic communications, all of them at the eastern end of the survey region. The instruments were spaced approximately 20 km apart, and were deployed along a 180 km long E-W transect, and two 100 km long N-S transects spaced ∼70 km apart. The registered time series were visually inspected for quality, tilt-corrected, rotated to the magnetic north, and finally windowed with data from two separate remote references. The GEOMAR instruments did not have compasses, so we used B_y-minimization to perform the rotation to the magnetic north, and for remote referencing we used a nonadjacent marine station as well as concatenated data from two land-based long period MT stations from the ATLAS experiment (Figure 1). The WHOI instruments did have compass information for the magnetic north rotation, and for the remote referencing we used a marine station and the

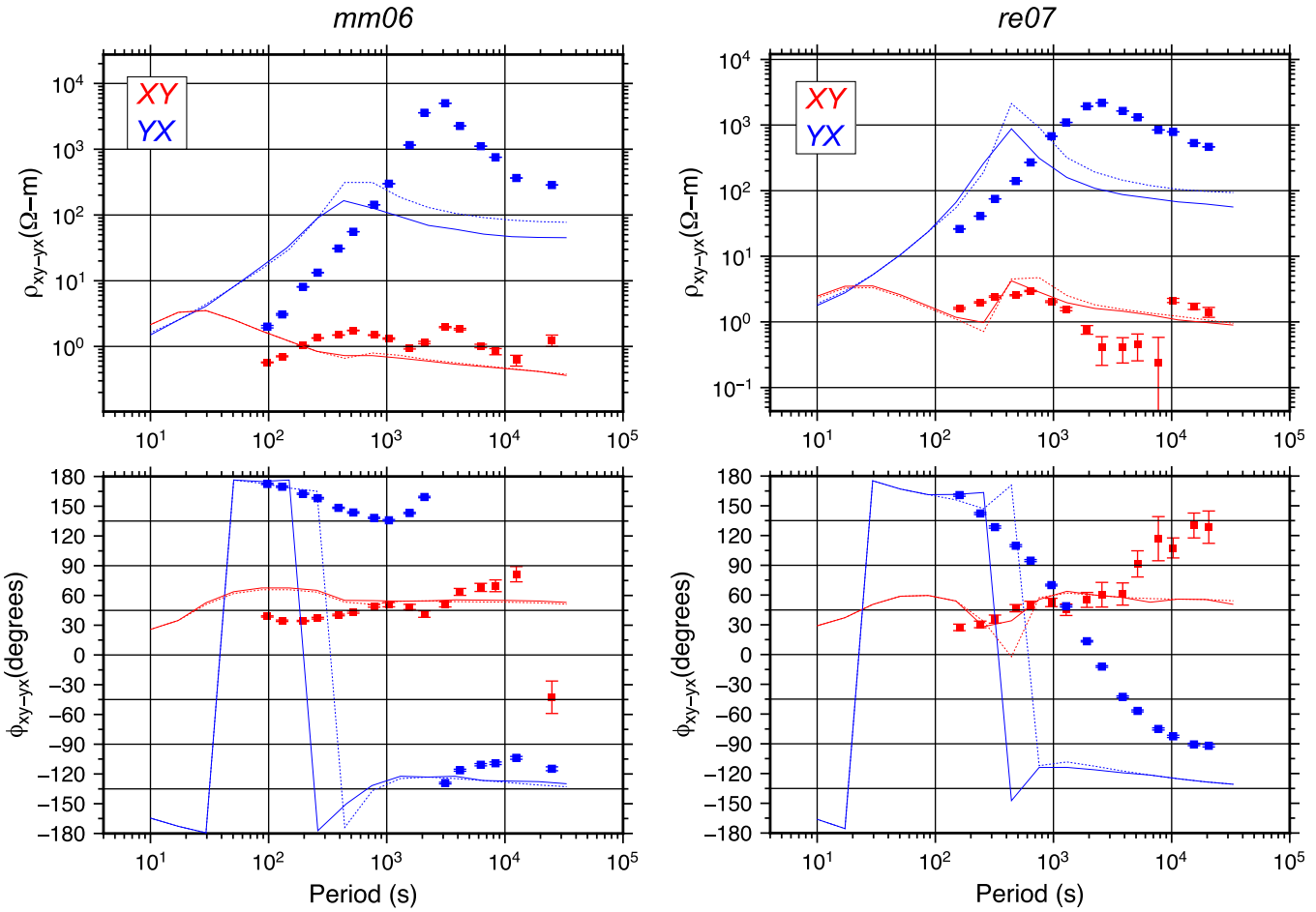

Figure 2. An example of marine data from the Alboran Sea showing the complex, 3-D characteristics of the MT response functions. Also shown are the responses of the starting model with (dashed line) and without (solid lines) conductive sediments in the Atlantic, west of Gibraltar. All seafloor responses are impacted by this large conductive feature and it is included in subsequent inversion models. Blue corresponds to the YX component and red to the XY component. Apparent resistivities and phases from (left) site MM06 and (right) site RE07. As is the common convention in MT, X indicates the North direction (abscissa), and Y the East direction (ordinate).

INTERMAGNET observatory station in Ebro, Spain. These time series were processed using the robust bounded influence remote reference processing (BIRRP) algorithm [*Chave and Thomson*, 2004], providing useful MT and tipper responses from 100 s up to greater than 30,000 s.

We are currently reprocessing all the time series available using a new algorithm [*Neukirch and Garcia*, 2014], which provides more reliable responses at longer periods that will allow us to obtain better images of the deeper structures.

3. Data Analysis

The marine data (15 MMT sites) show complex MT response functions with strong distortion due to seafloor topography [e.g., *Baba and Seama*, 2002; *Baba and Chave*, 2005] and the coast effect [e.g., *Key and Constable*, 2011; *Worzewski et al*., 2012], suggesting at least a moderately resistive lithosphere beneath the seafloor (Figure 2). The sharp peak in resistivity at around 300 s is a clear indication of coastal effects, as is the rolling of the phase. All elements of the impedance tensor are of comparable size (i.e., there is no rotation direction in which the diagonal elements of the tensor are substantially smaller than the off-diagonal elements as would be expected over structure with 2D-like characteristics). The land data used in the analysis were a subset, chosen on the basis of long-period (over 100 s if possible) data quality, of those already discussed in *Rosell et al*. [2011] where readers can find details of acquisition and processing.

The 3-D nature of both land and marine MT datasets, the close proximity of two complex coastlines and a rugged seafloor bathymetry, made 3-D inversion the only viable tool to obtain an electrical resistivity model

of the lithosphere beneath the northern branch of the Gibraltar arc, comprising the Alboran sea and the Betics. It would not have been possible, for example, to remove the effects of seafloor bathymetry from the data [e.g., *Baba and Chave*, 2005] to permit inversion over a flat seafloor, while maintaining the coastline geometry and including land data in the analysis.

Despite recent advancements in 3-D inversion of MT data [*Siripunvaraporn*, 2012], surprisingly few 3-D codes were available to us for handling such a complex data set.

4. 3-D Modeling

All the 3-D inversions were carried out using on the 3-D nonlinear conjugate gradient (NLCG) algorithm [*Mackie and Madden*, 1993; *Rodi and Mackie*, 2001] as implemented by Schlumberger. The algorithm minimizes the misfit between observed and computed data, using the framework of Tikhonov regularization [*Tikhonov and Arsenin*, 1977]. The code uses a regularization operator to produce a smoothly varying resistivity volume. The code is essentially the same as that used by *Burd et al.* [2013], although in our case the requirement to include land and marine data made the process more complex and computationally expensive.

An independent inversion of the land sites alone was first carried out in order to constrain the shallow structure beneath the Betics area derived from the higher frequencies available in the land data not included in the subsequent joint land-marine inversion. The resulting model was used as a preliminary model for the inversion of land and marine sites. To construct this preliminary model, a homogeneous model (100 Ohm-m) which included topographic changes on land and which also included the ocean (0.33 Ohm-m) and an approximate seafloor bathymetry was used as a starting model. Twenty-six periods were inverted between 0.1 s and 10,000 s, using errors floors of 3% for the apparent resistivity and phases of the off-diagonal elements of the impedance tensor (Zxy and Zyx), and 10% for the diagonal elements of the impedance tensor (Zxx and Zyy). The inversion converged after 46 iterations with a root mean square (RMS) value of 2.62. The responses of the final model match the data well at all sites. The model contains the same primary features as that obtained by *Rosell et al*. [2011], particularly the deep NS oriented conductor, which was the primary feature of discussion by those authors.

From this preliminary model, the next step was to generate the starting model to be used for the inversion of the 13 MT and 15 MMT sites. This was done by running intensive forward modeling to verify mesh parameters, particularly for sites on the seafloor, and resistivity contrasts. Different factors were tested, especially the size of the cells in the central part of the mesh, the resistivity values of the sediments of the Alboran sea, and the presence and influence of the sediments of the Atlantic Ocean. Bathymetry was determined using the GEBCO08 database [*GEBCO*, 2008] and the thickness of sediments beneath the Alboran was determined from seismic reflection data [*Soto et al*., 2008].

The area of investigation, both onshore and offshore, contains great topographic and bathymetric variations, from 2500 m above mean sea-level (AMSL) in the Betic Chain to −2000 m in the deepest parts of the Alboran Sea. In the central part of the mesh the cell size is 2 km × 2 km horizontally with 50 m thickness from sea-level to a depth of 2000 m, necessary to accurately capture the bathymetric variations and their impact on the MT responses. The topography was constructed using a cell size increasing from 50 m thick at sea-level to 200 m thick at 2500 m. This cell size was found to optimize mesh dimension (computation time) and precision of the forward modeling. Laterally and vertically the mesh was greatly extended to meet the boundary and continuity conditions needed to accurately calculate the forward model. The resulting mesh contains 3.3 million cells (159 x 186 x 111).

Below the seafloor the presence of conductive sediments had to be imposed, since the frequency range of our seafloor data cannot resolve shallow structures. The distribution of sediments in the Alboran Sea was constructed using sediment thickness imaged by seismic reflection surveys [*Soto et al*., 2008]. Several values of resistivity for the sediments between 0.4 Ohm-m and 2 Ohm-m were tested. In the end, we used a gradient, with resistivity increasing with depth, with values chosen in the way that were best able to reproduce the responses of the observed seafloor data at periods around 30 s.

The northern part of the African continent, the Atlantic Ocean and the Mediterranean Sea were included in our starting model (the actual extent of the 3-D mesh is marked in blue in the inset plot of Figure 1). The sediments of the Atlantic Ocean were also included. Sediment thickness reaches more than 5000 m close to the

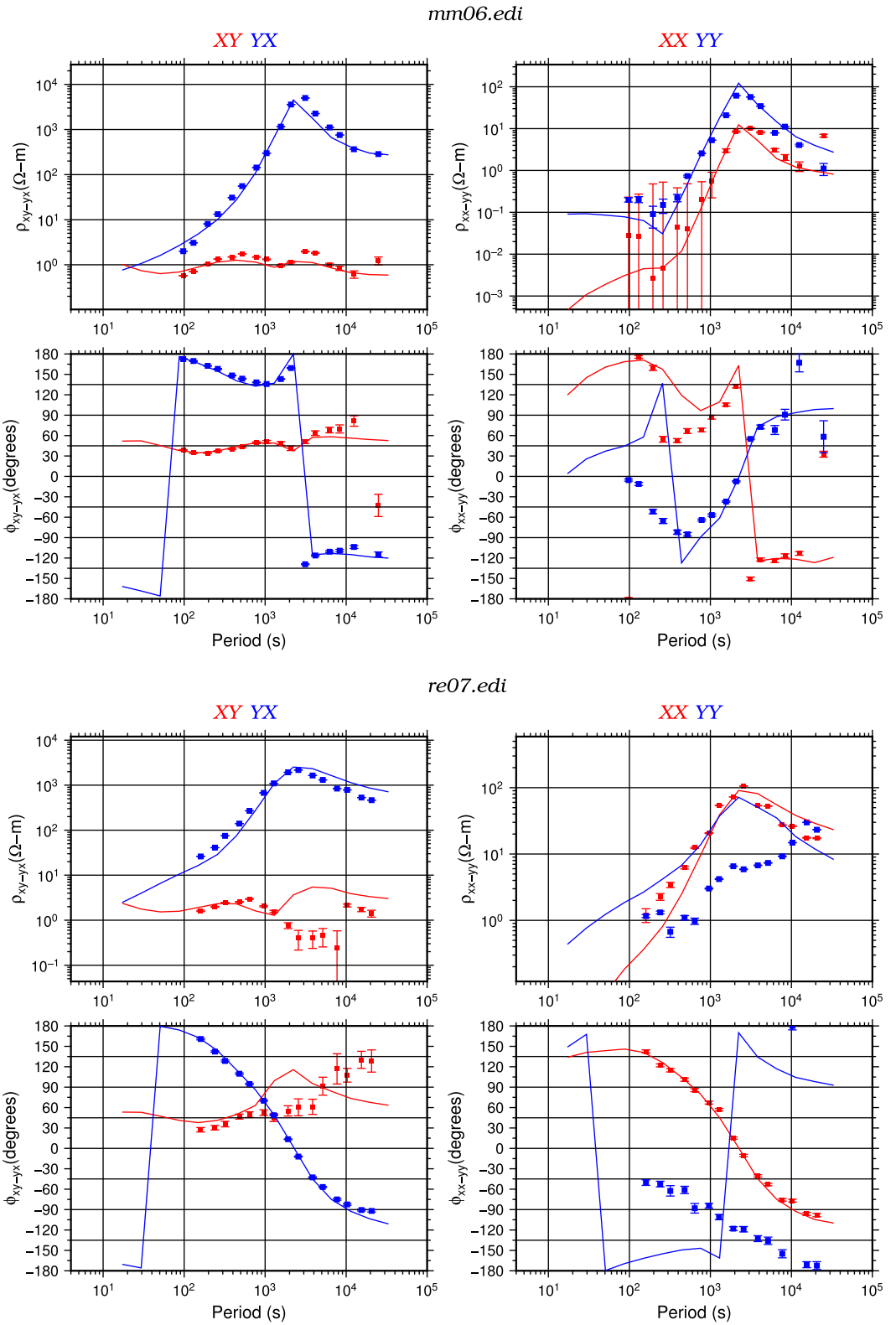

Figure 3. Example fits of the final inversion model for MMT data at the same sites as in Figure 2.

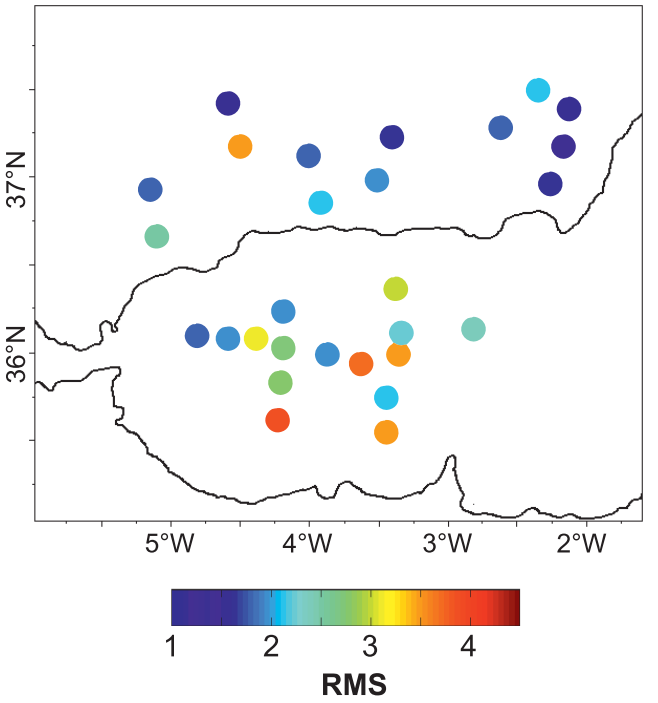

Figure 4. A map showing the RMS misfit of the final model at all sites included in the inversion.

Gibraltar Strait (online data of the *National Oceanic and Atmospheric Administration (NOAA)* [*Divins*, 2003]) at a distance around 150 km from the closest MMT site. The presence of this thick wedge of sediment affected most of the MMT sites at periods greater than ~100 s, particularly for the YX polarization. Figure 2 shows the responses of the starting model including the sediments (dotted line) compared to the same model without sediments (solid line). The sites located onshore were unaffected by the presence of the sediments.

These forward modeling tests were performed in order to start the inversion with a model that was already able to reproduce key response features related to the coast and bathymetric effects. This process allowed us to incorporate features that are known into the inversion, to account for first order distortions in the data related to the very strong coast effect in this region and seafloor bathymetry and, as a result, to make the inversion process more efficient. The starting model reproduces the cusps of the YX polarization associated with the complex coast effect [*Worzewski et al*., 2012; *Key and Constable*, 2011], the depressed XY polarization, and the phases out of quadrant in the responses. An example of this features can be found in Figure 2, where off-diagonal elements from sites mm06 and re07 show cusps at 300 s and phases rolling out of quadrant around 30 s, with a depressed XY polarization. The observed diagonal elements of these sites are shown in Figure 3.

5. MT/MMT Inversion

The full impedance tensor and the Tipper tensor were inverted at 28 sites. Sixteen frequencies between 10 s and 33,000 s were included. We applied errors floors equal to 1.5% for the off-diagonal components of the impedance tensor (0.87 degrees for the phases and 3% for apparent resistivity), and 10% to the diagonal components (5.73 degrees for the phases and 20% for the apparent resistivity). We applied an absolute error of 0.05 to the tipper. The running time was on average of about 40 min per iteration. For the inversion process we used a cluster with 30 nodes of 12 core CPUs each with 64 GB of RAM per node.

Our experience with this data set is that most of the information is contained within the MT responses functions. For this reason, the inversion was run in two steps: (1) inversion of the impedance tensor for 40 iterations, (2) inversion of the impedance tensor jointly with the magnetic transfer function until convergence (25 more iterations). In total the inversion iterated 65 times to convergence, reaching a final RMS of 2.3.

The responses of the final model fit the data well at all sites with no obvious regions that are poorly fit. Figure 3 shows the model response and observed data fit for two selected sites. Figure 4 shows a map of misfit for each of the stations included in the inversion. Figures 5 and 6 show the final model as a block and slices. Supporting information S1 and S2 contain the individual visual fits of the modeled impedance and tipper to the observations.

Four prominent features can be clearly seen in the final model (Figures 5a and 5b): (1) the presence of a moderately conductive zone (C4) below a strong resistive body (R1), that starts at 150 km depth and which extends to the base of the mesh; (2) a moderate conductor in the central part of the Alboran Sea (C1)

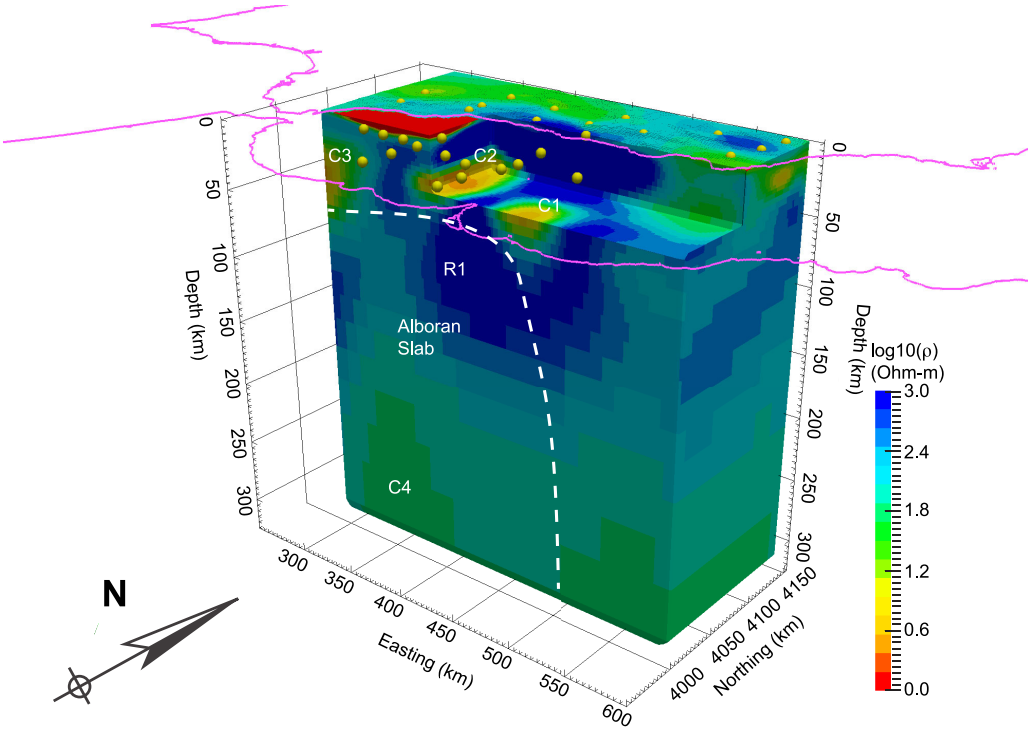

Figure 5. An E-W cross section through the final inversion model along the main EW marine profile. The four conductive and the resistive features discussed in the text are as labeled. The estimated location of the Alboran slab has been obtained from *Bezada et al*. [2013] and *Palomeras et al*. [2013]. The geographical projection used is a WGS84 zone 30.

(below sites mm05, mm06, re07, re11 and ns01) that extends from below the sediments to a depth of ~40 km just above the central part of the resistive zone R1; (3) a NS oriented conductor (C2), extending from the Betics to the Alboran Sea starting at ~20 km depth, and plunging to the north, reaching a depth of ~60 km below the coast. An additional conductor (C3), which is not tightly constrained by our data but nevertheless seems to be a required feature, is located West of the survey area under the Gibraltar Arc.

6. Sensitivity Tests

Sensitivity tests of the three main features discussed were carried out in order to prove that they are not simple artifacts of the inversion process or the result of fitting noise in the data. First of all, it is important to notice that all the inversion runs, using different regularization parameters, converged to final models that contained the same three structures discussed above. This repeatability already gives us great confidence that the model structure is robust. Sensitivity testing was done by removing each of the conductors separately, substituting them by resistivity values commensurate with the surrounding model structure. We carried out both forward modeling of the perturbed models to see the difference in responses with and without the conductive features, as well as using these perturbed models as starting models for new inversions, examining whether the original features returned. We assess the results of these tests qualitatively, comparing the responses of the final and perturbed models and looking at the reinverted models, and quantitatively comparing the root mean square (RMS) values for each site for each test. For the quantitative analysis we introduce a term that defines the change in the fitting of our data, for each site and each frequency. We refer to this term as the "update" and define it as:

$$Update(\%) = 100 \times \frac{RMS - RMS_0}{RMS_0},$$

where RMS is the RMS of the perturbed model and RMS_0 is the RMS of the final model. A positive update corresponds to a worsening of the data fit with respect to the original model.

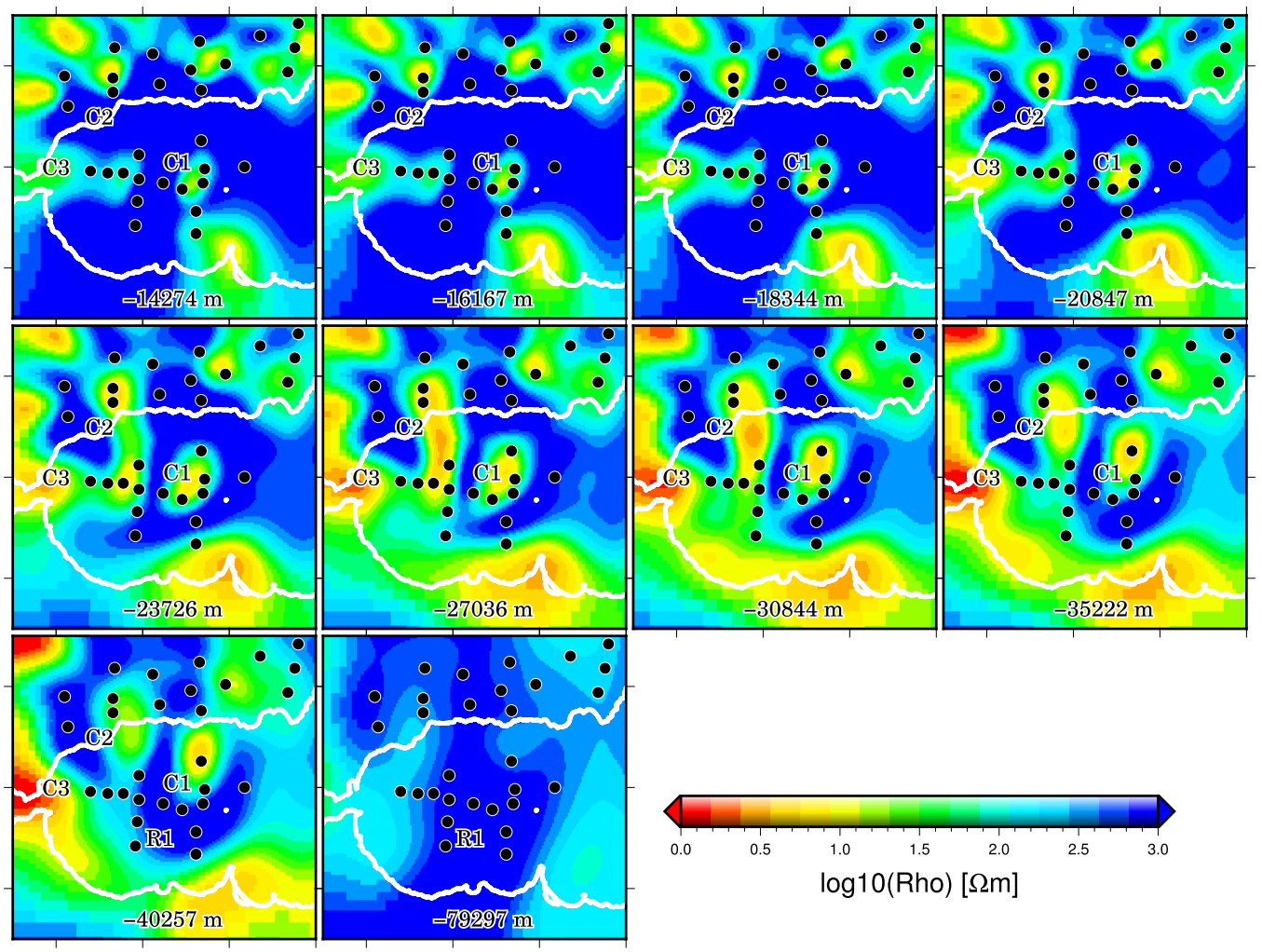

Figure 6. From Left to right and top to bottom, slices correspondent to depth levels 85–93 and level 98. The depth to the top of the slice is indicated within each plot. Conductive features C1, C2, and C3 and resistive Feature R1 discussed in text are as labeled.

During the inversion process we saw that the inclusion of the Tipper data did not greatly impact the resulting model: including the Tipper conserved all the structures present in the model obtained by inverting only the impedance tensor. We conclude from this observation that the inversion was driven primarily by the impedance tensor (even though the Tipper data, which contain significant structure, are well fit by our final inversion model). We thus performed the sensitivity tests using a higher error floor for the Tipper (0.2), in order to focus the tests on the changes related to the changes in the fitting of the impedance tensor.

6.1. Test 1

The transition to a lower resistivity mantle occurs around 150 km depth with values of around 100 Ohm-m observed (Feature C4 in Figures 5 and 6). We raised the resistivity of this region to 600 Ohm-m, a value that corresponds to the value of the resistive body located immediately above it. We are thus essentially testing whether the resistive body could extend deeper into the mantle. The forward modeling of this test showed a worsening of the data fit for all the MMT sites at long periods, especially in the YX polarization. The map showing the updates of the model after the forward modeling of the perturbed model (Figure 7a) highlights this worsening, with greater than 10% changes in the RMS for all the MMT sites. Inversion of the perturbed model did not recover the initial structure, but was also not able to significantly lower the starting RMS, suggesting that the inversion process became trapped in a local minimum. We feel that these tests confirm that the presence of a moderately low resistivity layer ($<$100 Ohm-m) between 120 and 150 km depth is required by the data.

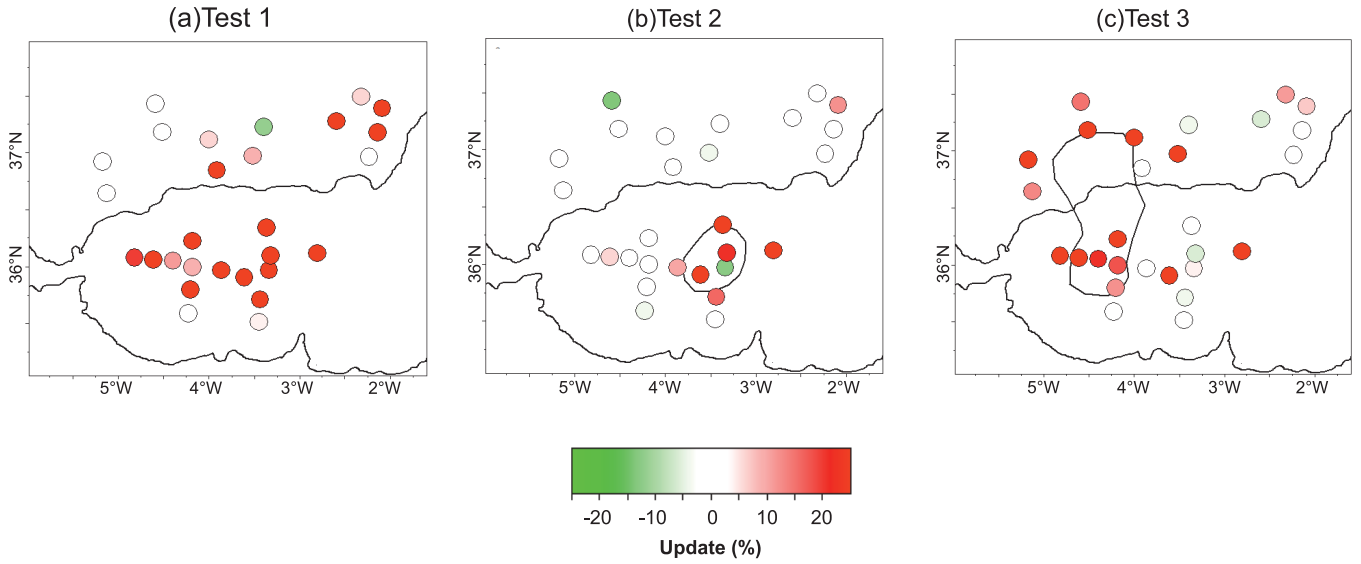

Figure 7. An update map for the three sensitivity tests discussed in the text. The black continuous line represents the shape of the anomaly tested at a depth of 40 km: (b) C1 and (c) C2.

6.2. Test 2

The anomaly C2 has a resistivity of about 5 Ohm-m, and was substituted by the surrounding resistivity in this area (500 Ohm-m). The forward modeling showed a significant worsening of the data fit for the sites located above the anomaly (Figure 7b). The responses were mainly affected in the period range from 20 to1000 s, especially for the XY polarization.

The inversion of the perturbed model converged quickly (after 12 iterations), but again was not able to reach the same RMS as the final inversion. However, the inversion reintroduced a conductive feature at the same location, albeit at a slightly higher resistivity value. Figure 8a shows the original model, and Figure 8b shows the model recovered after removing the anomaly. A depth slice view and an EW profile section is shown to highlight the lateral extent and depth of the conductor. The presence of a conductive body (resistivity $<\sim$10 Ohm-m) dipping north is well constrained by our inversion.

6.3. Test 3

Anomaly C1 has resistivity values between 5 and 10 Ohm-m. As for the previous tests, a resistivity value close to 500 Ohm-m was used to substitute the conductor. Forward modeling of the perturbed model shows a worsening of the data fit for both land MT and MMT sites located above and close to the anomaly (Figure 7c). Again, responses of this perturbed model differ from those of the original in the 20–1000 s period range, especially for the XY polarization. Inversion of the perturbed model converged after 16 iterations, without reaching an RMS comparable to the original inversion. The conductor returned in the model, however, although at a slightly greater depth than in the original model. The new feature also has a slightly different shape, especially in its extension to the north (see Figure 8c).

7. Discussion

The four primary features in our model can each be related to a subduction history for the Alboran Domain. The deep, vertical resistor in the mantle beneath the Alboran Sea relates directly to a high seismic velocity feature that extends to at least 300 km depth [*Bezada et al.*, 2013]. This feature has been interpreted as a vertical dipping slab plunging into the mantle, and such a feature is also consistent with SKS splitting data [*Alpert et al.*, 2013]. In our case, the decrease in resistivity at a depth of $\sim$150 km (Feature C4 in Figure 5) could be interpreted either as a termination of the slab or as a change in properties of the slab material. The former interpretation is at odds with seismic evidence and the reduction in resistivity is not sufficient to unequivocally call for a transition to asthenosphere. A change in the properties of the subducting Alboran slab has been proposed by *Gràcia et al.* [2003].

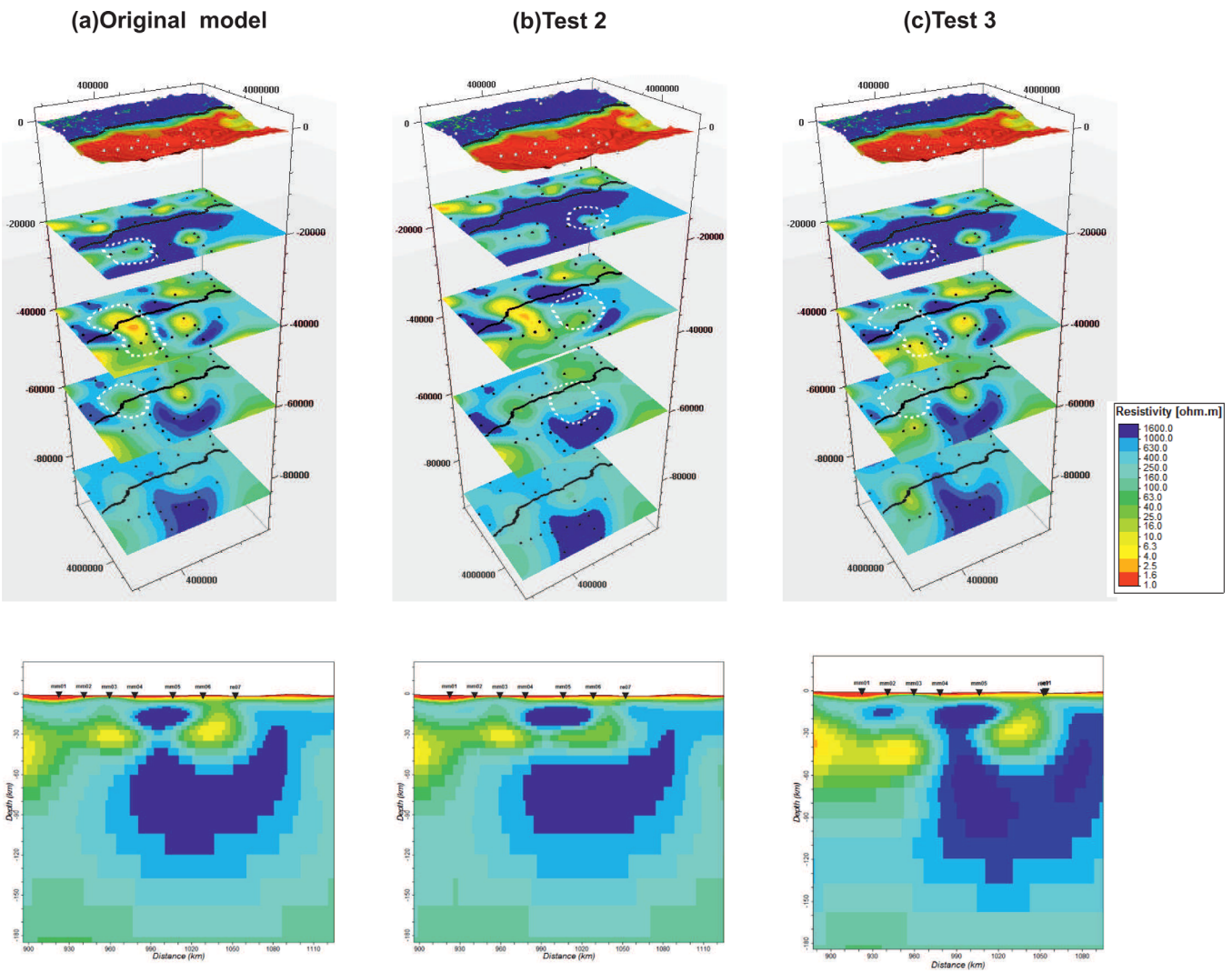

Figure 8. (top) Depth slices through the 3-D models (original and perturbed) and (bottom) corresponding cross sections along an EW line passing through the MMT sites. (a) The final inversion model. (b) The model resulting model obtained after reinverting, using a starting model in which the shallow conductor associated with Neogene volcanics (C1) was removed. The white-dashed line represents the shape of the original anomaly. (c) Same as Figure 8b but for the removal of the conductive feature interpreted as a tear in the slab (C2).

Values of typical asthenospheric resistivity at a depth of ~150 km appear, from deep probing soundings in the oceans, to be around 30–50 Ohm-m [*Sarafian et al.*, 2015]. A value of ~100 Ohm-m would be consistent with a dry, low oxygen fugacity (fO_2) asthenosphere, which is plausible, but appears not to be typical. Results from the Atlas Mountains to the south show resistivity values of ~100–150 Ohm-m in the upper-mantle which have been interpreted as lithospheric and not asthenospheric [*Kiyan*, 2015]. A reanalysis of teleseismic data, incorporating more arrivals into the modeling, apparently images a change in velocities in the downgoing slab at a similar depth to the observed change in resistivity [Max Bezada, Pers. Comm.]. In velocity images, this transition looks like a hole in the slab, but is most likely a change in the material that was subducted. A slightly damper lithospheric slab would be consistent with the change in resistivities we observe. Our data are not able to image a deeper increase in resistivity that would mark the transition back to dry slab at greater depth in accordance with seismic imaging.

The conductor associated with Neogene volcanics is also identifiable as a subduction related feature (Feature C1 in Figure 5). The location of the conductor is just to the east of the downgoing slab, and likely results from the release of fluids from the slab as it descends, with subsequent vertical migration of fluids and possible melt generation, as has been seen in electrical resistivity images at several subduction zones

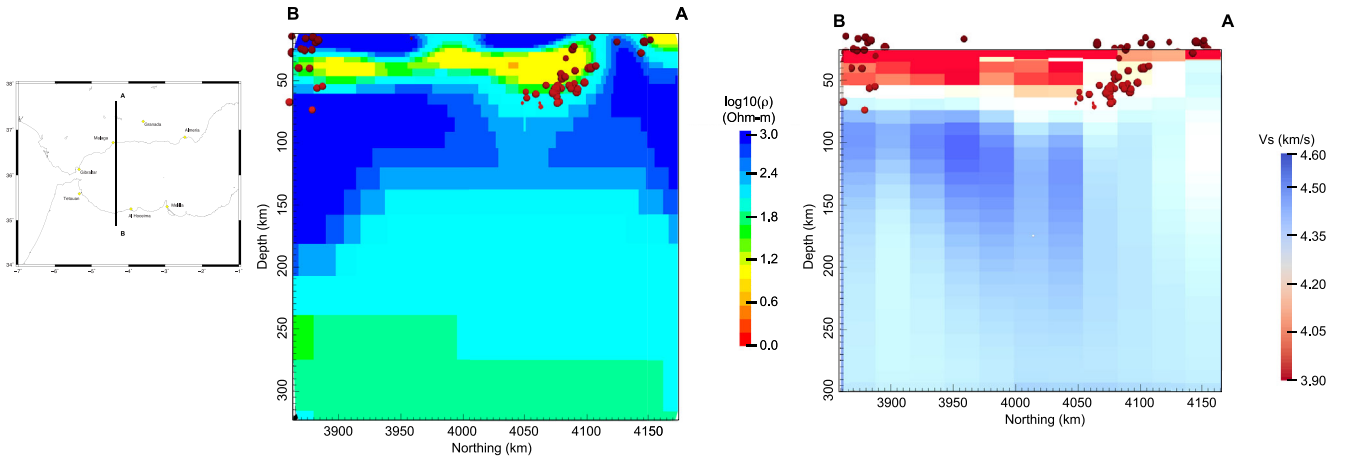

Figure 9. (middle) Detailed slice of the MT 3-D block at the area where the inland upper mantle conductor is located [*Rosell et al*., 2011]. (right) Rayleigh wave tomography from *Palomeras et al*. [2013] showing the coincidence velocity and resistivity of the Lithosphere properties in Alboran. The red-scaled dots are earthquakes (IGN database [*IGN*, 2015]) with easting restricted to the same location of the MT model cut. The projection used in the plot is WGS84 zone 30.

[e.g., *Worzewski et al*., 2010; *Matsuno et al*., 2010; *Evans et al*., 2014; *McGary et al*., 2014; *Wannamaker et al*., 2014]. In this case, unfortunately, we do not have sufficient data coverage (both in terms of frequency and spatially) to well constrain the geometry and fluid content of the feature. The upwelling of the fluids appears to be controlled by the boundary of the African plate to the southwest, which appears as a dipping resistive contact at the location of the Nekkor fault on the seafloor. The conductor sits beneath a region of thin crust where the moho is ∼20 km [*Thurner et al*., 2014]. The Neogene volcanics are consistent with shallow melting processes [*Thurner et al*., 2014]. The presence of melt in the upper mantle in this region would be consistent with high seafloor heatflow values which are seen through most of the eastern Alboran Basin [*Polyak et al*., 1996].

Another conductive feature speaks to the separation between the slab and continental lithosphere (Feature C2 in Figure 5). In an earlier paper, *Rosell et al*. [2011] interpreted a conductor in a similar location as due to a tear in the subducting slab that allowed asthenospheric material to flow upward. That analysis did not include seafloor data and so the extent of the conductor beneath the Alboran Sea was unconstrained. Seismic data from the region show changes in velocity in the same area as the conductor [*Palomeras et al*., 2014; *Thurner et al*., 2014] (Figure 8, right). Rather than a tear in the slab, *Thurner et al*. [2014] suggest a separation between the top of the slab and continental lithosphere that results in lateral asthenospheric flow. The gap could be related to delamination of continental lithosphere. Importantly, we note that the base of the conductor is coincident with a band of earthquake epicenters (Figure 9). Given the depth of the base of the conductor (∼40 km), the coincidence with the inferred top of the slab from seismic data [*Thurner et al*., 2014] and the band of seismicity, we suggest that the conductor represents fluids released from the slab due to the transition of basalt to eclogite. Similar fluid release has been seen in other subduction settings [e.g., *Worzewski et al*., 2010; *Evans et al*., 2014; *McGary et al*., 2014] at a similar depth. It is possible that these fluids migrate upward along the base of the overlying lithosphere and form the slightly shallower conductor seen beneath land to the north.

A final feature that can be recognized in our model is located to the West, under the Gibraltar Straight (Feature C3 in Figure 5). Although we do not have sufficient site coverage in this region to properly resolve this feature, the anomaly is robust and required by the inversion. *Palomeras et al*. [2014] image a low velocity feature at the same location, on top of the Alboran slab.

8. Conclusions

We have collected a complex marine MT data set from the Alboran Sea in the western Mediterranean. The data are highly three-dimensional in form and required a fully 3-D inversion treatment incorporating

seafloor bathymetry and coastline geometry in order to properly capture first order distortion effects on the data. Despite the significant distortion, through careful inversion of both land and marine MT data, we have been able to constrain primary features in the mantle that point to a complex subduction history for the region. These features include two conductors we interpret as caused by the release of fluids from the subducting slab. The other feature is a resistive body associated with a near vertically plunging slab beneath the Alboran as has been imaged seismically.

Acknowledgments

This project was initiated as a result of and supported by NSF project-EAR080-9074 (Evans, lead P.I.) and Spanish National Projects CTM2009-07039-E/MAR, CTM2011-30400-C02-02 and Repsol funded CO-DOS project. We would like to thank Chris Judge, Maik Neukirch, Rafael Bartolomé, and Manel Prada for their assistance at sea. Imma Palomeras is thanked for making the Rayleigh tomography available to us. Manel Fernandez is thanked for making the Alboran sediment thickness data available to us. Some figures have been made using the GMT package [*Wessel and Smith*, 1991] and Paraview [*Ahrens et al*., 2005]. The Barcelona Center for Subsurface Imaging is a Grup d'Excel·lència de Qualitat (ref. 2014 SGR 940). The Geomodels Research Institute and the Research Group of Geodynamics and Basin Analysis is a Grup d'Excel·lència de Qualitat (ref. 2014 SGR 467). The Marine MT data are available from the authors upon request (revans@whoi.edu). Earthquake database for Alboran downloaded from the web page of the Instituto Geografico Nacional in 2015 (http://www.ign.es/ign/layoutIn/sismoFormularioCatalogo.do). The authors would like to acknowledge the insightful reviews by editor Thorsten Becker and two anonymous reviewers.

References

Ahrens, J., B. Geveci, and C. Law (2005), *ParaView: An End-User Tool for Large Data Visualization*, Visualization Handbook, Elsevier, Burlington, Mass., doi:10.1016/B978-012387582-2/50038-1.

Alpert, L. A., M. S. Miller, T. W. Becker, and A. A. Allam (2013), Structure beneath the Alboran from geodynamic flow models and seismic anisotropy, *J. Geophys. Res. Solid Earth*, *118*, 4265–4277, doi:10.1002/jgrb.50309.

Amaru, M. L. (2007), Global travel time tomography with 3-D reference models, PhD thesis, *Geol. Ultraiectina*, *274*, 174.

Baba, K. (2005), Electrical structure in marine tectonic settings, *Surv. Geophys.*, *26*(6), 701–731, doi:10.1007/s10712-005-1831-2.

Baba, K., and A. D. Chave (2005), Correction of seafloor magnetotelluric data for topographic effects during inversion, *J. Geophys. Res.*, *110*, B12105, doi:10.1029/2004JB003463.

Baba, K., and N. Seama (2002), A new technique for the incorporation of seafloor topography in electromagnetic modeling, *Geophys. J. Int.*, *150*, 392–402, doi:10.1046/j.1365-246X.2002.01673.x.

Bezada, M. J, E. D. Humphreys, D. R. Toomey, M. Harnafi, and J. M. Dávila and J. Gallart (2013), Evidence for slab rollback in westernmost Mediterranean from improved upper mantle imaging, *Earth Planet. Sci. Lett.*, *368*, 51–60, doi:10.1016/j.epsl.2013.02.024.

Burd, A. I., J. R. Booker, R. Mackie, C. Pomposiello, and A. Favetto (2013), Electrical conductivity of the Pampean shallow subduction region of Argentina near 33S: Evidence for a slab window, *Geochem. Geophys. Geosyst.*, *14*, 3192–3209, doi:10.1002/ggge.20213.

Chave, A. D., and D. J. Thomson (2004), Bounded influence magnetotelluric response function estimation, *Geophys. J. Int.*, *157*(3), 988–1006, doi:10.1111/j.1365-246X.2004.02203.x.

Chertova, M. V., W. Spakman, T. Geenen, A. P. van den Berg, and D. J. J. van Hinsbergen (2014), Underpinning tectonic reconstructions of the western Mediterranean region with dynamic slab evolution from 3-D numerical modeling, *J. Geophys. Res. Solid Earth*, *119*, 5876–5902, doi:10.1002/2014JB011150.

Divins, D. L. (2003), *Total Sediment Thickness of the World's Oceans & Marginal Seas*, NOAA Natl. Geophys. Data Cent., Boulder, Colo.

Evans R., L., P. E. Wannamaker, R. S. McGary, and J. Elsenbeck (2014), Electrical structure of the central Cascadia subduction zone: The EMSLAB Lincoln Line revisited, Earth Planet. *Sci. Lett.*, *402*, 265–274, doi:10.1016/j.epsl.2013.04.021.

Filloux, J. H. (1980), North Pacific magnetotelluric experiments, *J. Geomag. Geoelectr.*, *32*, suppl. 1, Sl33–Sl43, doi:10.5636/jgg.32.Supplement1_Sl33.

García-Castellanos, D., and A. Villaseñor (2011), Messinian salinity crisis regulated by competing tectonics and erosion at the Gibraltar arc, *Nature*, *480*(7377), 359–363, doi:10.1038/nature10651,.

GEBCO (2008), The GEBCO_08 Grid, version 20090202. [Available at http://www.gebco.net.]

Gràcia, E., J. Dañobeitia, J. Vergés, R. Bartolomé, and D. Córdoba (2003), Crustal architecture and tectonic evolution of the Gulf of Cadiz (SW Iberian margin) at the convergence of the Eurasian and African plates, *Tectonics*, *22*(4), 1033, doi:10.1029/2001TC901045.

Gutscher, M.-A., J. Malod, J.-P. Rehault, I. Contrucci, F. Klingelhoefer, L. Mendes-Victor, and W. Spakman (2002), Evidence for active subduction beneath Gibraltar, *Geology*, *30*, 1071–1074, doi:10.1130/0091-7613-31.1.e22.

Key, K. (2012), Marine electromagnetic studies of seafloor resources and tectonics, *Surv. Geophys.*, *33*(1), 135–167, doi:10.1007/s10712-011-9139-x.

Key, K., and S. Constable (2011), Coast effect distortion of marine magnetotelluric data: Insights from a pilot study offshore northeastern Japan, *Phys. Earth Planet. Inter.*, *184*, 194–207, doi:10.1016/j.pepi.2010.11.008.

Kiyan, D. (2015), Multidimensional magnetotelluric imaging of crustal and uppermost mantle structures of the Atlas Mountains of Morrocco, PhD thesis, NUI Galway, Ireland.

Lonergan, L., and N. White (1997), Origin of the Betic-Rif mountain belt, *Tectonics*, *16*, 504–522, doi:10.1029/96TC03937.

Mackie, R. L., and T. R. Madden (1993), Three-dimensional magnetotelluric inversion using conjugate gradients, *Geophys. J. Int.*, *115*, 215–229, doi:10.1046/j.1365-246x.2000.00007.x.

Mancilla, F. L., D. Stich, M. Berrocoso, R. Martin, and J. Morales (2013), Delamination in the Betic Range: Deep structure, seismicity and GPS motion, *Geology*, *41*(3), 307–310, doi:10.1130/G33733.1.

Matsuno, T., et al. (2010), Upper mantle electrical resistivity structure beneath the central Mariana subduction system, *Geochem. Geophys. Geosyst.*, *11*, Q09003, doi:10.1029/2010GC003101.

McGary, R. S., R. L. Evans, P. E. Wannamaker, J. Elsenbeck, and S. Rondenay (2014), Pathway from subducting slab to surface for melt and fluids beneath Mount Rainier, *Nature*, *511*(7509), 338–340, doi:10.1038/nature13493.

Miller, M. S., A. Allam, T. W. Becker, J. F. DiLeo, and J. Wookey (2013), Constraints on the geodynamic evolution of the westernmost Mediterranean and northwestern Africa from shear wave splitting analysis, *Earth Planet. Sci. Lett.*, *375*, 234–243, doi:10.1016/j.epsl.2013.05.036*375*.

Naif, S., K. Key, S. Constable, and R. L. Evans (2013), Melt-rich channel observed at the lithosphere-asthenosphere boundary, *Nature*, *495*, 356–359, doi:10.1038/nature11939.

Neukirch, M., and X. Garcia (2014), Nonstationary magnetotelluric data processing with instantaneous parameter, *J. Geophys. Res. Solid Earth*, *119*, 1634–1654, doi:10.1002/2013JB010494.

Palomeras, I., S. Thurner, A. Levander, K. Liu, A. Villasenor, R. Carbonell, and M. Harnafi (2014), Finite-frequency Rayleigh wave tomography of the western Mediterranean: Mapping its lithospheric structure, *Geochem. Geophys. Geosyst.*, *15*, 140–160, doi:10.1002/2013GC004861.

Platt, J. P., and R. L. M. Vissers (1989), Extensional collapse of thickened continental lithosphere: A working hypothesis for the Alboran Sea and Gibraltar Arc, *Geology*, *17*, 540–543, doi:10.1130/0091-7613(1989)017<0540:ECOTCL>2.3.CO;2.

Platt, J. P., W. M. Behr, K. Johanesen, and J. R. Williams (2013), The Betic-Rif arc and its orogenic hinterland: A review, *Annu. Rev. Earth Planet. Sci.*, *41*, 313–357, doi:10.1146/annurev-earth-050212-123951.

Polyak, B. G., et al. (1996), Heat flow in the Alboran Sea, western Mediterranean, *Tectonophysics*, *263*, 191–218, doi:10.1016/0040-1951(95)00178-6.

Rodi, W., and R. L. Mackie (2001), Nonlinear conjugate gradients algorithm for 2-D magnetotelluric inversions, *Geophysics*, *66*, 174–187, doi: 10.1190/1.1444893.

Rosell, O., A. Marti, A. Marcuello, J. Ledo, P. Queralt, E. Roca and J. Campanya (2011), Deep electrical resistivity structure of the northern Gibraltar Arc (western Mediterranean): Evidence of lithospheric slab break-off, *Terra Nova*, *23*, 179–186, doi:10.111/j.1365-3121.2011.00996.x.

Sarafian, E., R. L. Evans, J. Collins, J. Elsenbeck, G. Gaetani, J. Gaherty, G. Hirth, and D. Lizarralde (2015), The electrical structure of the Central Pacific upper mantle constrained by the NoMelt experiment, *Geochem. Geophys. Geosyst.*, *16*, 1115–1132, doi:10.1002/2014GC005709.

Siripunvaraporn, W. (2012), Three-dimensional magnetotelluric inversion: An introductory guide for developers and users, *Surv. Geophys.*, *33*(1), 5–27, doi:10.1007/s10712-011-9122-6.

Soto, J.-I., F. Fernández-Ibáñez, M. Fernàndez, and A. Garcia-Casco (2008), Thermal structure of the crust in the Gibraltar Arc: Influence on active tectonics in the western Mediterranean, *Geochem. Geophys. Geosyst.*, *9*, Q10011l, doi:10.1029/2008GC002061.

Spakman, W., and M. J. R. Wortel (2004), Tomographic view on western Mediterranean geodynamics, in *The TRANSMED Atlas, The Mediterranean Region From Crust to Mantle*, edited by W. Cavazza et al., pp. 31–52, Springer, Berlin.

Strack, K. M. 2014), Future directions of electromagnetic methods for hydrocarbon applications, *Surv. Geophys.*, *35*(1), 157–177, doi: 10.1007/s10712-013-9237-z.

Thurner, S., I. Palomeras, A. Levander, R. Carbonell, and C.-T. Lee (2014), Ongoing lithospheric removal in the western Mediterranean: Evidence from Ps receiver functions and thermobarometry of Neogene basalts (PICASSO project), *Geochem. Geophys. Geosyst.*, *15*, 1113–1127, doi:10.1002/2013GC005124.

Tikhonov, A. N., and V. Y. Arsenin (1977), *Solutions of Ill-Posed Problems*, V.H. and Sons, Washington, D. C.

van Hinsbergen, D. J. J., R. L. M. Vissers and W. Spakman (2014), Origin and consequences of western Mediterranean subduction, rollback and slab segmentation, *Tectonics*, *33*, 393–419, doi: 10.1002/tect.20125.

Wannamaker, P. E., R. L. Evans, P. A. Bedrosian, M. J. Unsworth, V. Maris, and R. S. McGary (2014), Segmentation of plate coupling, fate of subduction fluids, and modes of arc magmatism in Cascadia, inferred from magnetotelluric resistivity, *Geochem. Geophys. Geosyst.*, *15*, 4230–4253, doi:10.1002/2014GC005509.

Wessel, P., and W. H. F. Smith (1991), Free software helps map and display data, *Eos Trans. AGU*, *72*, 441–446, doi:10.1029/90EO00319.

Wortel, M. J. R., and W. Spakman (2000), Subduction and slab detachment in the Mediterranean-Carpathian region, *Science*, *290*, 1910–1916, doi:10.1126/science.290.5498.1910.

Worzewski, T., M. Jegen, H. Kopp, H. Brasse, and W.T. Castillo (2010), Magnetotelluric image of the fluid cycle in the Costa Rican subduction zone, *Nat. Geosci.*, *4*, 108–111, doi:10.1038/NGEO1041.

Worzewski, T., M. Jegen and A. Swidinsky (2012), Approximations for the 2D coast effect on marine magnetotelluric data, *Geophys. J. Int.*, *189*, 357–368, doi:10.1111/j.1365-246X.2012.05385.x.